Incomplete Peierls-like chain dimerization as a mechanism for intrinsic conductivity and optical transparency: A La-Cu-O-S phase with mixed-anion layers as a case study

Jino Im, Giancarlo Trimarchi, Kenneth Poeppelmeier, and Alex Zunger

Phys. Rev. B **92**, 235139 — Published 22 December 2015

DOI: 10.1103/PhysRevB.92.235139

An incomplete Peierls-like chain dimerization as a mechanism for intrinsic conductivity and optical transparency: a La-Cu-O-S phase with mixed-anion layers as a case study

Jino Im[1], Giancarlo Trimarchi[1], Kenneth Poeppelmeier[2], and Alex Zunger[3]

[1]*Dept. of Physics, Northwestern University, 2145 Sheridan Road, Evanston, IL*

[2]*Dept. of Chemistry, Northwestern University, 2145 Sheridan Road, Evanston, IL*

[3]*University of Colorado, Renewable and sustainable Energy Institute Boulder, Colorado*

The family of La-based copper oxide sulfides includes LaCuOS, the prototypical transparent conducting oxide sulfide when doped, as well as $La_5Cu_6O_4S_7$ a compound with a layered structure analogous to LaCuOS but with a row of O atoms substituted by S atoms in the LaO layer. We propose that $La_5Cu_6O_4S_7$ is the first instance of an oxide-sulfide *intrinsic* transparent conductor (i.e., not requiring doping).Such a 1D chain feature in related systems often promotes a Peierls distortion with respect to the equispaced chain whereby adjacent atoms form dimers, a distortion that is expected to lead to the opening of a band gap and the lowering of the total energy, thus to thermodynamic stability. In $La_5Cu_6O_4S_7$ we find that the configuration with undimerized 1D chains (the α phase) is both metallic and thermodynamically unstable. The fully dimerized, Peierls configurations (the β phase) exhibits an insulating band gap, however it is energetically unstable. The stable structure has chains with a ~66 % degree of dimerization; in this structure the energetically preferred repeating chain motif is one in which two dimers are separated by one S atom, while chain segments with directly adjacent dimers are energetically unfavorable. The stable configuration is metallic with electron depletion in the Cu_2S_2 layer with respect to the Cu d^{10} valence configuration that effectively amounts to creating a hole in the Cu bands that the valence maximum. In the stable partially dimerized phase the intra-band, plasmonic transitions are weak while the onset of the strong inter-band transitions is at around 3 eV which are both properties that enable transparency. In this paper we explain (i) why $La_5Cu_6O_4S_7$ has an incomplete Peierls distortion, (ii) how the incomplete Peierls distortion in $La_5Cu_6O_4S_7$ creates the unusual coexistence of transparency and conductivity, producing what appears to be the first oxide-sulphide intrinsic transparent conductor, (iii) discuss the agreement between the predicted and the measured structure.

1. Introduction

Transparent conductors (TCs) are initially transparent insulators that are rendered conducting by the addition of either *n*-type or *p*-type dopant atoms.[1-8] An example of such chemically doped TCs is LaCuOS[9-15] (see Figure 1(a)), which is the prototypical *p*-type transparent conducting oxide sulfide when doped. However, most materials in thermodynamic equilibrium can usually tolerate only a limited density of *extrinsic* dopants before secondary phases start to precipitate, whereas the tolerance to *intrinsic* defects is limited by the eventual occurrence of structural instability[9-11]. Furthermore, the enrichment of the system by added electrons or holes produced by doping can also lower the formation energy of the intrinsic defects of the opposite charge sign (e.g., oxygen vacancy donors can form spontaneously in intentionally hole doped oxides[11, 12]), thus limiting the carrier concentration that can be achieved. Recently, a new paradigm for *intrinsic* transparent conducting materials has been advanced[16] in which intentional, extrinsic doping is not required. Instead, one starts with a metal that already has plenty of free carriers, and achieves transparency by designing a band structures that permit but *weak* inter-band transitions in the visible range, and has only low energy and weak intra-band plasmonic excitations.[17] Examples of such recently proposed (Ref 16) metallic bulk ceramics include *n*-type $Ag_3Al_{22}O_{34}$ and $Ba_3Nb_5O_{15}$, and *p*-type $Rb_4Nb_{11}O_{30}$.

Here, we propose the first *intrinsic* hole transparent conductor in a layered oxide-sulfide, specifically $La_5Cu_6O_4S_7$,[18-22] having, in addition, a new mechanism based on remarkable deviations from the standard Peierls dimerization expected in regular one dimensional systems. This compound was observed[18] to have the layered structure shown in Figure 1(b). Unlike LaCuOS, $La_5Cu_6O_4S_7$ has a row of S atoms substituting a row of LaO_2 units in the La_2O_2 layer creating a *quasi 1D chain* (see Figure 1(c). This chain makes different the in-plane lattice parameters of the so-obtained standalone La and Cu layers. This misfit

is accommodated by a slight compressive distortion in the Cu layer that brings the La and Cu layers to be commensurate. In the limiting case of undimerized, equispaced S chain, the S *p* orbitals would produce a half filled 1D metallic electronic band (see Fig. 2(a)). This should instigate a Peierls distortion that will produce a dimer chain while opening a gap and stabilizing the chain by decreasing its total energy.[23] This dimerization ideally occurs in (pseudo-)1D systems in which the only band crossing the Fermi level is that originating from the overlap of orbitals in the 1D chain *and* this 1D band is half-filled. Based on our DFT calculated band structure (see details in section III) of the undimerized configuration of the misfit compound with equispaced chains displayed in Fig. 2(a) we observe that this phase does not meet these conditions for the standard Peierls dimerization: First, along with a band originating from the 1D S chain there are also other bands originating in the Cu_2S_2 layer that traverse the Fermi level. Second, the 1D S band is more than half-filled (i.e., ~70 % filled). Therefore, the configuration with fully dimerized chains would not be expected *a priori* to be stable in this misfit oxide sulfide. We have therefore investigated various energy-lowering atomic displacements. The calculations of the DFT total energy as a function of the chain dimer density (see Fig. 3) confirm that neither the undimerized nor the dimerized forms are the ground-state structure. Surprisingly, we find that the dimerized phase is also higher in energy than the undimerized one. The energetically favorable structure is, instead, one with ~66% dimer density in the partially dimerized S chains (γ phase). Interestingly, we find that the γ phase has an unusually weak optical absorption in the visible range (*nearly transparent*) due to weak dipole transitions between occupied valence states and unoccupied mid-gap states originating from the S-*p* chain orbitals. We show that as a result of the partial dimerization the Cu_2S_2 layer gets partially depleted of electrons to maintain the overall charge neutrality, with the result of rendering the Cu_2S_2 layer, and the whole system, a hole conductor. We propose that in the thin film form the La-O-Cu-S misfit phase is a possible *p*-type transparent conductor being also the first instance of an oxide-sulfide semi-transparent conductor without doping.

In this paper we will explain (i) why $La_5Cu_6O_4S_7$ has an incomplete Peierls distortion, (ii) how the incomplete Peierls distortion in this misfit oxide sulfide creates the unusual coexistence of transparency and conductivity, producing what appears to be the first oxide-sulphide *intrinsic* transparent conductor, (iii) discuss the agreement between the predicted and the measured structure. We envisage other examples of phases with a similar structural feature that produces intrinsic transparent conductivity could be identified in the structurally flexible family of layered oxide chalcogenides.

II. The experimentally characterized crystal structure

The XRD experiments performed by Chan *et al.* (Ref.[21]) revealed that $La_5Cu_6O_4S_7$ forms in a layered crystal structure (see Fig. 1(b)) analogous to the structure of LaCuOS (see Figure 1(a)). There are two alternating layers in $La_5Cu_6O_4S_7$: a Cu_2S_2 layer, with the PbO-type fluorite structure in which the Cu atoms form the central sheet of the layer, and a mixed oxide-sulfide La_5O_4S layer, with an anti-PbO-type structure in which the anions form the central sheet. The La_5O_4S layers can be derived from the anti-PbO-type La_2O_2 layers of LaCuOS by substituting one row of LaO_2 units every six with one row of S atoms. The crystal structure refinement shows that this substitution has the effect of decreasing the in-plane *b* lattice parameter from 16.955 Å in LaCuOS to 15.757 Å in $La_5Cu_6O_4S_7$ creating compressive sinusoidal-like ripples in the Cu_2S_2 layer along the *b* direction, as well as expanding the out-of-plane *c* lattice parameter from 17.035 Å to 17.550 Å. The crystal structure refinement shows that the S chains as formed by "split sites". Each split site *n* consists of the two positions A_n and B_n. Each site *n* is occupied by only one S atom that takes with equal probability one of the two available positions as shown in Fig. 1(c). As a result the split positions at adjacent sites *n* and $n+1$ can be occupied with the following possible combinations: (i) B_n and A_{n+1} are occupied forming a *dimerized* pair with an observed distance of 2.106 Å; (ii) A_n and A_{n+1} (or B_n and B_{n+1}) are occupied forming an *undimerized* pair with an observed distance of 2.834 Å long; (iii) A_n and B_{n+1} are occupied forming a *broken-bond* pair with an observed distance of 3.555 Å. The experimental observations show that the chain is partially dimerized, thus comprised between the two limits of fully ordered configurations, i.e., the equispaced (α phase) and fully dimerized (β phase) chains. However, the experiments that were performed could not give indications on what is the dimer frequency and whether there are regular patterns in the way the dimers and undimerized atoms distribute on the chain. In this study, we investigated the stability and electronic structure of various realizations of partially dimerized configurations to identify the stable chain pattern and its band structure properties.

III. Total energy and band structure of the various chain configurations

We modeled the α (undimerized) and β (dimerized) phases in the experimentally refined unit cell (see Fig. 1(c)) which includes two split sites per chain. To model the partially dimerized chains we used supercells built repeating the experimentally observed unit cell, which contains 44 atoms, two, three, and four times along the chain direction thus simulating supercells including up to 176 atoms. In each supercell we studied all the distinct chain configurations that can be generated by occupying the split-site positions included in the supercell. The pseudopotential density-functional total energy and force method as implemented in the VASP code[24, 25] was used to relax all atom coordinates in each configuration to the energy minimum. The *initial* configurations for each structural relaxation are set by occupying one of the two available positions at each site as show in Fig. 1(b). The X-Ray diffraction measurements indicate the dimers so defined are not tilted, thus we didn't

add tilting to the dimers. After structural relaxation we find that the dimers didn't undergo tilting.

The band structures shown in Fig. 2 for the various chain configurations were calculated using the semilocal generalized gradient approximation exchanged and correlation functional in the PBE formulation.[26] In the optical properties calculations discussed in Sec. IV, we used the Heyd-Scuseria-Ernzerhof (HSE) hybrid functional[27] in the HSE06[28] formulation to correct the band gap and the position of the conduction bands of the chain configurations that have a band gap at the GGA level. Via HSE we calculated the valence-to-conduction energy distance at the Gamma point and then shifted the GGA conduction bands so as to match the HSE energy distance.

A. The undimerized metallic α phase is energetically unstable

The undimerized configuration (the α phase) was generated by placing the S atoms only at the A or the B positions of every split site, with an initial (later relaxed) nearest-neighbor distance a_{chain}=2.834 Å equal to the experimentally measured distance between the split sites. In this configuration there is the forces on the chain atoms have a zero component along the chain that as a result remains equispaced upon structural optimization. Fig. 2(a) shows the metallic electronic band dispersion of the undimerized configuration along the Γ-to-X direction in the Brillouin zone (BZ) parallel to the 1D Sulphur chains in reciprocal space and with the X point at the zone boundary. The radius of the *red* markers is proportional to the projection of the wave functions on the S p_x atomic orbitals aligned to the chain direction. (See the full band structure and projected density of states shown in the Supplementary Information, Figure S1(a).) The S p_x orbitals produce a 1D-like band[29] along Γ-to-X. The Fermi level cuts this 1D band at k_F = 0.599 π/a_{lat} along Γ-to-X. Recall that the band structure is calculated using the experimental crystallographic cell which has a lattice parameter along the chain twice longer than the lattice parameter of the undimerized chain. By unfolding the 1D band to the BZ of the undimerized and regularly spaced S chain (which has the a_{chain} spacing), we obtain $k_F \approx 0.7005 \times (\pi/a_{chain})$ which implies that the 1D chain band is more than half-filled. Because the 1D chain band is more than half-filled and is not the only band crossing the Fermi level, the conditions for the chain stabilization via the Peierls dimerization mechanism are not met. The total energy calculations discussed in the next sections (see Fig.3) elucidate the stability of the dimerized phase with respect to the undimerized and partially dimerized phases.

B. The fully Peierls-dimerized β phase is also unstable and higher in energy than the undimerized metallic α phase

We performed a total-energy calculation with the restriction to full uniform dimerization. This configuration was set up by occupying the B_n and A_{n+1} positions at adjacent split sites in the experimentally observed cell. This phase is insulating as illustrated by the band structure in Fig. 2(b) along Γ-to-X (the full band structure is shown in Fig. S1(b) in the Supplementary Information), but is higher in energy than the undimerized α phase (see Fig. 3). The effect of the dimerization is the opening of a ~5 eV gap at the point $X=\pi/(2a_{chain})$, which is the BZ boundary point of the regular dimer chain. The upper branch of the 1D band before dimerization (see Fig. 2(a)) is partially occupied and moves completely into the conduction as a result of the large gap opening due to the dimerizaton. Also as a result of the dimerization the electrons in excess of half-filling transfer to the hole-like pockets at the top of the Cu-S band manifold. The projected density of states on the valence atomic orbitals for the misfit oxide sulfide shown in Figure S1 of the Supplementary Information is analogous to the prototype LaCuOS[12] oxide sulfide in which the valence band originated from the interaction between Cu-d and S-p levels and for which it was shown[12, 30] that the states at the top of the valence band are mostly of Cu-*d* origin and antibonding. Thus after the dimerization the Cu atoms can be described by a closed-shell d^{10} configuration. We will examine next the *partially* dimerized phase and the mechanism that makes it stable with respect to the α and β phase.

C. The partially dimerized γ phase is the ground state structure

C.1 The experimentally observed structure

The crystal structure measurements indicate that the S chains are partially dimerized. However these measurements could not determine the frequency of the dimers along the chain nor whether there is a periodic or recurring stable pattern formed by the dimers. We therefore performed DFT total energy calculations to determine the dimer density and possible recurring chain motifs that are associated to the energetically stable chain.

C.2 Expectations from the general Peierls model for k_F away from half-filling

Band theory asserts that the geometry of the Fermi surface is a predictor of the atom displacements that will emerge in a lattice so as to pre-empt electronic instabilities. Pseudo-1D metallic systems are thus assumed to be unstable with respect to a charge density modulation because the Fermi surface of a 1D system (it is a point) is always nested by the nesting vector $q=2k_F$ where k_F is the Fermi vector. The periodic lattice distortions that is coupled to the charge density modulation of wave vector q has periodicity $\lambda=2\pi/q=\pi/k_F$. This periodicity is a multiple of the undistorted chain lattice constant a_{chain} by a factor that can be rational (i.e., λ is commensurate to a_{chain}) or irrational (i.e., non-commensurate to a_{chain})[29, 31] depending on k_F. For example, the dimerization, which is the simplest case of Peierls distortion,[23, 32, 33] occurs in systems with half-filled bands where $k_F=0.5\times(\pi/a_{chain})$. In this case, upon the opening of a band gap there is the formation of dimers from neighboring atoms producing a modulation of periodicity $\lambda=\pi/k_F = 2a_{chain}$, i.e., double the periodicity of the equispaced chain.

As noted above, the metallic undimerized α phase with $k_F \approx 0.7005 \times (\pi/a_{chain})$ is away from half-filling. The q wave vector of the predicted periodic distortion (after reduction to the first Brillouin zone) is $q \approx 0.2995 \times (2\pi/a_{chain})$ to which it corresponds a wave-length $\lambda = 3.389 \times a_{chain}$. Therefore, the gap-opening distortion that would stabilize the chain is *incommensurate* with the undistorted, equispaced chain and should have a periodicity comprised between 3 and 4 times (in fact, closer to 3 times) the periodicity of the undimerized chain.

C.3 Total energy minimization assuming partial dimerization: the γ phase

***Structural model*:** To determine if there is a preferred dimer density in the partially dimerized chains, we simulated all the *distinct* (i.e., non-equivalent) partially dimerized configurations (Fig. 1(b)) that can be realized distributing the S atoms over the split sites within 2×1×1, 3×1×1, and 4×1×1 supercells built, respectively, repeating 2, 3, and 4 times the crystallographic unit cell along the chain direction. Each distinct chain arrangement is characterized by a dimer density x defined as the number of dimers in the starting configuration (before relaxation) divided by the total number of dimers that would form the ideal fully dimerized chain that fits the given supercell. Fig. 3 shows the total energy of the fully *relaxed* supercells as a function of the dimer density x and referred to the total energy of the undimerized configuration (which has x=0) which is set equal to zero. The formation energy of an isolated dimer can be estimated calculating the total energy difference between a supercell containing a single dimer and the same supercell with undimerized chains. Taking the 4×1×1 supercell, the largest supercell we considered in this study, with one dimer per cell (configuration 3) as an approximation for an isolated dimer we estimate a dimer formation energy of -20 meV per dimer.[34]

Stability of the partially dimerized configurations: The energetically favorable configuration among all the partially dimerized configurations is found in the 3×1×1 supercell and has a dimer density of x=0.66 (see Fig. 2(c), and also Fig. 3, panel 5). This configuration features a motif defined by one dimer 2.154 Å long followed by one undimerized S atom 3.175 Å away, and this motif repeats periodically. A higher energy configuration with x=0.66 (Fig. 3, panel 6) distinct from the previous one can be realized in a 3×1×1 supercell: this has two adjacent dimers each 2.200 Å long followed by a broken-bond pair with the S atoms 3.494 Å apart from each other. The configuration with x=0.33 that we calculated in the 3×1×1 supercell was unstable and relaxed into a configuration with x=0.66. This reflects the instability of a structure with a charge modulation that does not match the modulation predicted based on the band structure analysis for the undimerized configuration. In the 4×1×1 supercell two distinct configurations with x=0.75 can be realized, each including three dimers: a lower energy configuration (see Fig. 3, panel 7) that features two adjacent dimers, and a higher energy configuration (see Fig. 3, panel 8) with three adjacent dimers followed by a broken-bond pair.

Origin of the stable chain patterns: The total energy decreases as the dimer density increases starting from the undimerized configuration. This trend can be intuitively understood considering that the formation of new dimers produces an energy gain and stabilization. However, the total energy reaches a minimum at x=0.66 and increases again beyond this value reaching a maximum in correspondence of the fully dimerized configuration. A visual inspection of the energetically unfavorable configurations with x=0.66 and 0.75 points to the fact that they feature two or more contiguous dimers. This observation indicates that an energy price is indeed implied by having dimers contiguous to each other along the chain. The γ phase with x=0.66 is the one that affords the best compromise between maximizing the number of dimers along the chain and minimizing the number of adjacent dimers.

The stability of γ phase with the chain pattern shown in Fig. 3, panel 5 can be explained observing that the ideal, lattice-incommensurate charge modulation with wavelength $\lambda \approx 3.3389 \times a_{chain}$ is near to the lattice-commensurate periodicity $\lambda = 3 \times a_{chain}$. Thus, one would expect that the best way to fit the lattice-incommensurate chain modulation corresponding to the calculated k_F on a crystal that has the periodicity a_{chain} is to realize chain segments with the commensurate modulation $\lambda = 3 \times a_{chain}$ that are occasionally interrupted by regions in which this periodicity is missed. Fig. 4 shows a schematics of the charge modulation with $\lambda = 3 \times a_{chain}$: this modulation would produces an excess of valence charge with a maximum between two neighboring atoms inducing there the formation of a dimer; the minimum of charge occurs at the site between two dimers and the atom at this site would remain equidistant from the neighboring dimers. This is indeed the lattice distortion found in the lowest energy structure at x=0.66. We can then expect that on the mesoscopic scale the residual discommensuration due to the actual $\lambda \approx 3.3389 \times a_{chain}$ periodicity would be accommodated by short clusters of two or more dimers that occasionally interrupt longer chain segments with the commensurate $\lambda = 3 \times a_{chain}$ pattern we just described.

C.4 Intrinsic hole content in the γ phase

The ground-state γ phase has a metallic band structure (Fig. 2(c)) with the Fermi level right below the top of Cu_2S_2 valence manifold. In this partially dimerized configuration the Cu d states near to the top of the valence band partially empty and we can assign a $d^{10-\eta}$ orbital configuration to the Cu atoms with $0<\eta<1$. The system remains charge-balanced through the accumulation of electrons from the Cu layer into the S chains as evidenced by the S chain subbands that become occupied upon partial dimerization and are located within 2 eV from the Fermi level as shown by the projected band structure of Figure 2(c). It is worth noting that the electron charge that accumulates on the S chains occupies bands that are completely filled and far

from the Fermi level (see the projected Fig. 2(c) and the full band structure in Fig. S1(c) in the Supporting Information[35]) and that do not contribute to transport. *Thus the hole-like states localized in the Cu_2S_2 layer are responsible for the p-type metallic behavior of $La_5Cu_6O_4S_7$ that was experimentally reported*[18-20]. This is a highly desirable feature in the band structure to realize a *p*-type transparent conducting material.

IV. The optical properties of the semi-transparent metallic γ phase

Optical absorption measurements[21, 22] of $La_5Cu_6O_4S_7$ give an optical gap of 2.0 eV, meaning this compound as opposed to LaCuOS is only partially transparent to the visible light in its bulk form. Figure 5 shows the calculated absorption spectra α(ω) of $La_5Cu_6O_4S_7$ in the two configurations, respectively with fully dimerized chains and partially dimerized chains with dimer density x=0.66; these two spectra are compared with the spectrum calculated for LaCuOS. To calculate the optical absorption spectrum[36] of LaCuOS and of the β and γ phases of the misfit phase we shifted the GGA conduction bands by an amount determined via an HSE06 calculation performed on a regular k-point grid.[37] The optical absorption edge of LaCuOS is consistent with the experimental measurement with a predicted optical band gap of 3.0 eV. The misfit layered oxide sulfide in the fully dimerized β phase has a similar α(ω) profile as the prototypical oxide sulfide LaCuOS above 3 eV and most of the absorption occurs above this threshold. However, $La_5Cu_6O_4S_7$ in the x=0.66 partially dimerized configuration exhibits additional features that contribute to the absorption below this threshold. These features include a shoulder around 2.8 eV and small peaks around 2.0 eV and 1.5 eV that correspond to optical transitions between deeper occupied states in the valence band and the unoccupied bands in the hole-pocket.

While these additional transitions decrease the optical band gap with respect to that of LaCuOS, consistent with experimental measurement, they are weak enough to suggest the possibility of still obtaining a good degree of transparency for the misfit oxide sulfide in the thin-film form. Figure 5 (b) shows that those additional peaks are smaller than 1×10^4 cm^{-1}. Since the optical absorption coefficient α(ω) determines the transmittance[38] owing to its direct proportionality to the factor $e^{-\alpha(\omega)l}$, where l is the sample thickness, the calculated optical absorption coefficient of $La_5Cu_6O_4S_7$ implies that 100 nm thickness of the sample transmits over 90% of visible light, which points to the possibility of rendering $La_5Cu_6O_4S_7$ a *p*-type transparent conducting material with intrinsic carrier content due to the chain modulation.

V. Discussion and Conclusions

Through the identification of the stable partial chain pattern in the misfit oxide sulfide $La_5Cu_6O_4S_7$ and the analysis of its electronic structure, we uncovered a new mechanism for inducing an intrinsic hole content without extrinsic dopants or intrinsic defects that alter the nominal stoichiometry. However, the family of layered oxide-chalcogenides includes numerous other systems in which Cu_2Ch_2 layers (*Ch* is a chalcogen species) alternate with layers of various compositions and structure (see Clarke *et al*., Ref.[39]). It is conceivable that using growth methods under an excess of the chalcogen species one could obtain systems with mixed oxide-chalcogenide layers as the one that characterize $La_5Cu_6O_4S_7$. Moreover, changing the structure and composition of the oxide layer is a means to control the onset of optical absorption threshold, thus providing a knob to potentially design new intrinsic transparent conductors.

To conclude, in this paper we explained why the misfit layered phase in the La-Cu-O-S system, i.e., $La_5Cu_6O_4S_7$, has an incomplete Peierls distortion and compare the stable structure obtained by *ab initio* calculations with the experimental structure. Furthermore we explain how the incomplete Peierls distortion creates the unusual co-existence of transparency and conductivity in this misfit layered La-Cu-O-S phase, producing what appears to be the first oxide-sulphide intrinsic transparent conductor. We propose that $La_5Cu_6O_4S_7$ could be rendered a possible *p*-type transparent conductor in thin film form and it thus represents the first instance of an oxide-sulfide (semi-)transparent conductor without doping. It is conceivable that more examples of phases with a similar structural feature inducing intrinsic transparent conductivity could be identified in the structurally flexible class of layered oxide chalcogenide compounds.

Acknowledgments: The work of K.R.P. was supported in part by the U.S. Department of Energy (DOE), Basic Energy Sciences, Office of Science, under Contract DE-AC02-06CH11357. The work of A.Z. was supported by the DOE's Office of Science, Basic Energy Science, MSE division, via Grant DE-FG02-13ER46959. J.I. and G.T. used in this research resources of the National Energy Research Scientific Computing Center (NERSC), a DOE Office of Science User Facility supported by the Office of Science of the U.S. Department of Energy under Contract No. DE-AC02-05CH11231.

References

1. K. L. Chopra, S. Major and D. K. Pandya, Thin Solid Films **102** (1), 1-46 (1983).
2. I. Hamberg and C. G. Granqvist, Journal of Applied Physics **60** (11), R123 (1986).
3. H. Kawazoe, M. Yasukawa, H. Hyodo, M. Kurita, H. Yanagi and H. Hosono, Nature **389** (6654), 939-942 (1997).
4. J. Im, G. Trimarchi, H. Peng, A. J. Freeman, V. Cloet, A. Raw and K. R. Poeppelmeier, Journal of Chemical Physics **138** (19), 194703 (2013).
5. G. Trimarchi, H. Peng, J. Im, A. Freeman, V. Cloet, A. Raw, K. Poeppelmeier, K. Biswas, S. Lany and A. Zunger, Phys. Rev. B **84** (16), 165116 (2011).

6. S. Lany and A. Zunger, Physical Review Letters **98** (4), 2-5 (2007).
7. G. Hautier, A. Miglio, G. Ceder, G.-M. Rignanese and X. Gonze, Nature Communications **4**, 2292 (2013).
8. Ç. Kılıç and A. Zunger, Physical Review Letters **88** (9), 095501 (2002).
9. M. Palazzi, C. R. Acad. Sci. **292**, 789 (1981).
10. K. Ueda, S. Inoue, S. Hirose, H. Kawazoe and H. Hosono, Applied Physics Letters **77** (17), 2701-2703 (2000).
11. K. Ueda and H. Hosono, Journal of Applied Physics **91** (7), 4768-4770 (2002).
12. K. Ueda, H. Hosono and N. Hamada, Journal of Physics: Condensed Matter **16** (28), 5179-5186 (2004).
13. H. Kamioka, H. Hiramatsu, H. Ohta, M. Hirano, K. Ueda, T. Kamiya and H. Hosono, Applied Physics Letters **84** (6), 879-881 (2004).
14. H. Hiramatsu, H. Kamioka, K. Ueda, H. Ohta, T. Kamiya, M. Hirano and H. Hosono, Physica Status Solidi (a) **203** (11), 2800-2811 (2006).
15. K. Ueda, H. Hiramatsu, M. Hirano, T. Kamiya and H. Hosono, Thin Solid Films **496** (1), 8-15 (2006).
16. X. Zhang, L. Zhang, J. D. Perkins and A. Zunger, Phys. Rev. Lett. **115**, 176602 (2015).
17. M. Dressel and G. Gruener, *Electrodynamics of Solids*. (Cambridge University Press, Cambridge, UK, 2002).
18. F. Q. Huang, P. Brazis, C. R. Kannewurf and J. A. Ibers, Journal of Solid State Chemistry **155** (2), 366-371 (2000).
19. I. Ijjaali, K. Mitchell and J. A. Ibers, Journal of Solid State Chemistry **177** (3), 760-764 (2004).
20. M. L. Liu, L. B. Wu, F. Q. Huang, L. D. Chen and J. A. Ibers, Journal of Solid State Chemistry **180** (1), 62-69 (2007).
21. G. H. Chan, M.-l. Liu, L.-d. Chen, F.-q. Huang, D. E. Bugaris, D. M. Wells, J. R. Ireland, M. C. Hersam, R. P. V. Duyne and J. A. Ibers, Inorganic chemistry **47** (10), 4368-4374 (2008).
22. W. Libin, L. Minling, H. Fuqiang, C. Lidong and G. Xiangdong, Ceramics International **35** (6), 2509-2512 (2009).
23. R. Hoffmann, Angewandte Chemie International Edition **26** (9), 846-878 (1987).
24. G. Kresse and J. Hafner, Journal of Physics: Condensed Matter **6** (40), 8245 (1994).
25. G. Kresse and J. Furthmüller, Physical Review B **54** (16), 11169-11186 (1996).
26. J. P. Perdew, K. Burke and M. Ernzerhof, Physical Review Letters **77** (18), 3865-3868 (1996).
27. J. Heyd, G. E. Scuseria and M. Ernzerhof, Journal of Chemical Physics **118** (18), 8207-8207 (2003).
28. A. V. Krukau, O. A. Vydrov, A. F. Izmaylov and G. E. Scuseria, Journal of Chemical Physics **125** (22), 224106 (2006).
29. M.-H. Whangbo, edited by J. Rouxel (D. Reidel Publishing Company, Dordrecht, Holland, 1986), pp. 27-85.
30. K. Ueda, H. Hosono and N. Hamada, Journal of Applied Physics **98** (4), 043506-043506 (2005).
31. J. Rouxel, edited by J. Rouxel (D. Reidel Publishing Company, Dordrecht, Holland, 1986), pp. 1-26.
32. R. E. Peierls, *Quantum Theory of Solids*. (Clarendon, Oxford, 1964).
33. G. Gruener, *Density waves in solids*. (Addison-Wesley Publishing Company, 1994).
34. The comparison of the total energy of the configurations with x=0.66 in which the dimers are separated by one undimerized S atom (configuration 5) and nearest neighbors (configuration 6) indicates that there is an increase in energy when the dimers become nearest neighbors with a repulsion energy of ~ 40 meV. However, to calculate the interaction energy with confidence would require a supercell likely larger than the largest supercell (i.e., 4×1×1) we considered in this study.
35. See Supplemental Material at [LINK TO BE INCLUDED BY THE EDITOR] for further synthetic details. The Supplemental Material includes details of the theo-retical calculations and figures showing the full band structures of the three main phases discussed in the main text.
36. C. Ambrosch-Draxl and J. O. Sofo, Computer Physics Communications **175** (1), 1-14 (2006).
37. H. J. Monkhorst and J. D. Pack, Physical Review B **13** (12), 5188-5192 (1976).
38. P. Y. Yu and M. Cardona, *Fundamental of semiconductors*, Third Edition ed. (Springer, 2001).
39. S. J. Clarke, P. Adamson, S. J. C. Herkelrath, O. J. Rutt, D. R. Parker, M. J. Pitcher and C. F. Smura, Inorganic chemistry **47** (19), 8473-8486 (2008).

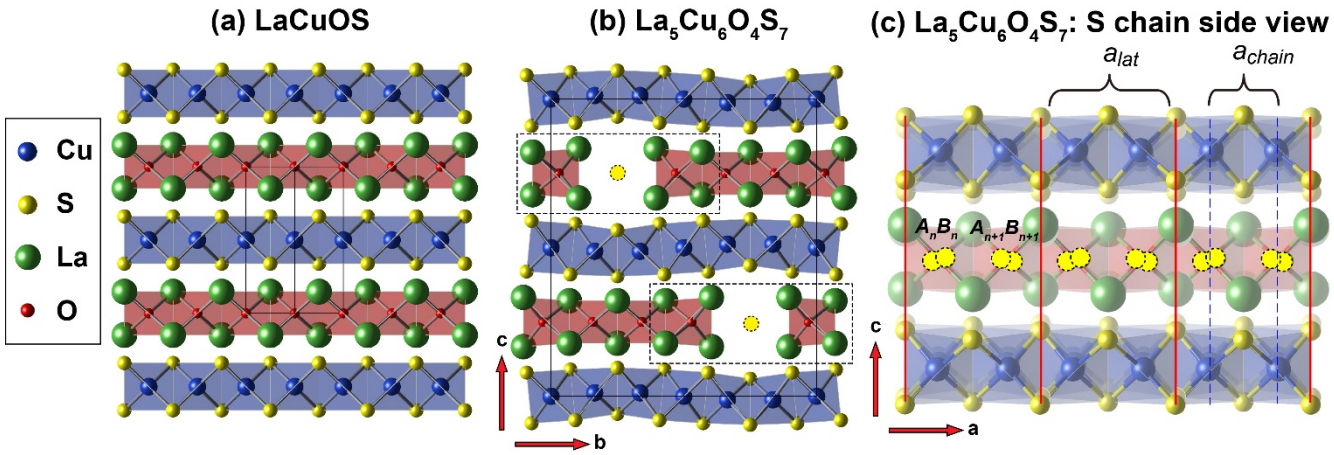

Figure 1. Experimental crystal structure of (a) LaCuOS (Ref. 9) and (b) $La_5Cu_6O_4S_7$ (Ref. 18) The two structures are shown along the (100) direction and the sections that are displayed comprise the same number Cu_2S_2 units along the *b* axis to facilitate a side-by-side comparison of the two structures. The unit cell of $La_5Cu_6O_4S_7$ includes 44 atoms. (c) Side view of the $La_5Cu_6O_4S_7$ experimental structure along the direction of the 1D sulphur chains in the La_5O_4S layers. These chains are sequences of "split sites" each consisting of a pair of positions. Each site *n* is occupied by only one S atom that takes with equal probability either of the split positions A_n or B_n. The lattice parameter a_{lat} of the crystallographic unit cell along the chain direction is twice the lattice spacing a_{chain} between split sites (it corresponds to the separation between the medium points of two adjacent sites *n* and *n+1*).

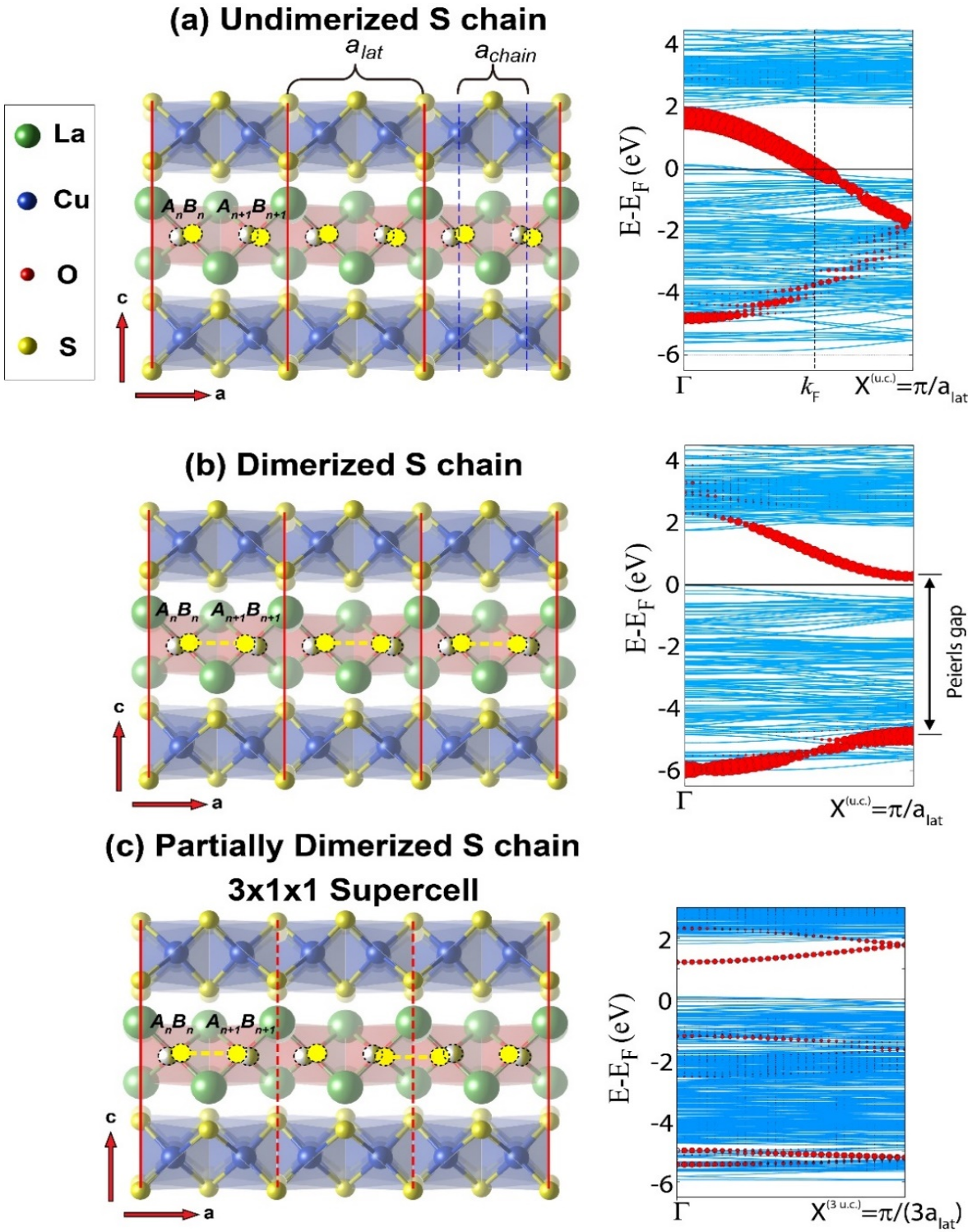

Figure 2. Band structure of the $La_5Cu_6O_4S_7$ misfit oxide sulfide in the configurations with (a) undimerized S chains (α phase), (b) fully dimerized S chains (β phase), and in the energetically favored (c) partially dimerized S chain configuration (γ phase) with dimer density x=0.66. The energy dispersion bands shown on the right hand side of each panel were calculated at the GGA-PBE level for the structure that was fully optimized with the same exchange and correlation functional. The radius of the red markers is proportional to the projection of the wave functions on the S p_x atomic orbitals aligned to the chain direction. The γ phase is the energetically most stable one (see Fig. 3) among all the distinct chain patterns that were investigated in supercells up to 4 times the crystallographic cell along the chain direction.

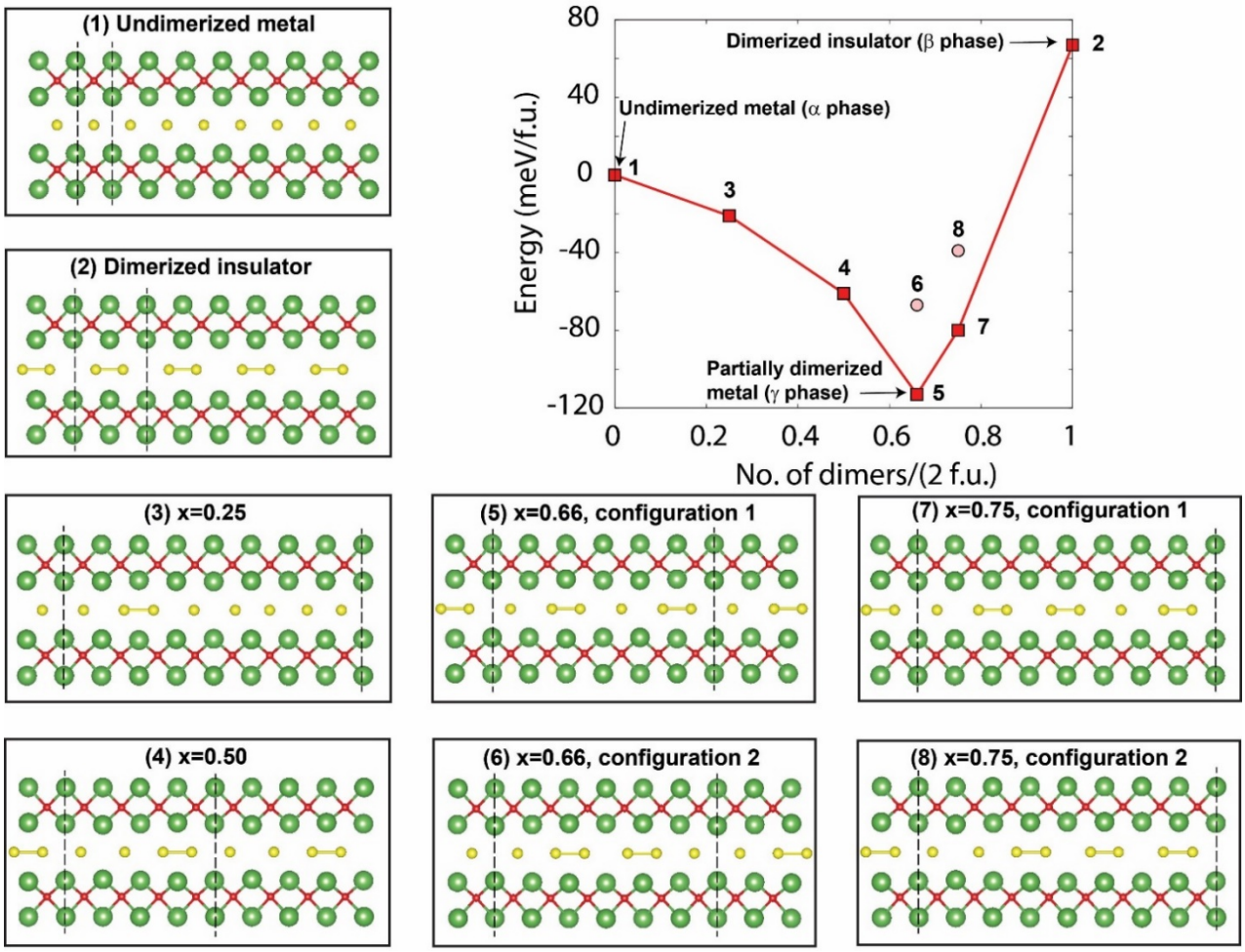

Figure 3. GGA-PBE total energy of the $La_5Cu_6O_4S_7$ misfit oxide sulfide calculated as a function of the dimer density x (defined in the main text) for all the distinct chain patterns that can be realized occupying the chain split sites (Fig. 1(c)) in supercells built repeating up to 4 times the crystallographic unit cell along the chain direction. The total energies (in eV per formula unit) are referred to the total energy of the undimerized configuration which is set equal to zero. Structure **1** and **2** correspond to the undimerized (x=0) and fully dimerized (x=1) chain configurations, respectively. Structure **3** is the configuration with x=0.25 realized in a 4×1×1 supercell and includes one dimer per chain within the supercell. Structure **4** is the configuration with x=0.5 realized in a 2×1×1 supercell and includes one dimer per chain within the supercell; two dimers along the chain are separated by a broken-bond pair. Structure **5** and **6** at x=0.66 (2/3) correspond to the two distinct chain configurations with this density that fit a 3×1×1 supercell, while structures **7** and **8** are the two distinct configuration with density x=3/4 that can be modeled in a 4×1×1 supercell.

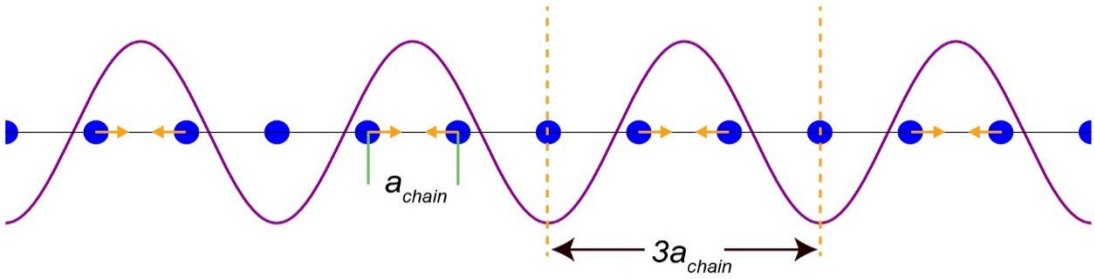

Figure 4. Schematic picture of a periodic row of atoms of lattice spacing a_{chain} with a commensurate charge modulation of wave length $\lambda=3\times a_{chain}$. The arrow centered at two adjacent atoms indicate the deformation of the chain to form a dimer in correspondence of a maximum of the charge. The atom between two distorted dimers remains equidistant from those dimers. This schematics depicts the charge modulation and the corresponding atom displacements that are one found in the predicted minimum energy γ phase with x=0.66. This commensurate modulation and atom distortion is a good approximation for the incommensurate modulation of wavelength $\lambda=2\pi/(2k_F)=3.3389\times a_{chain}$ that is predicted based on the Fermi vector k_F obtained in the band structure with undimerized chains (α phase).

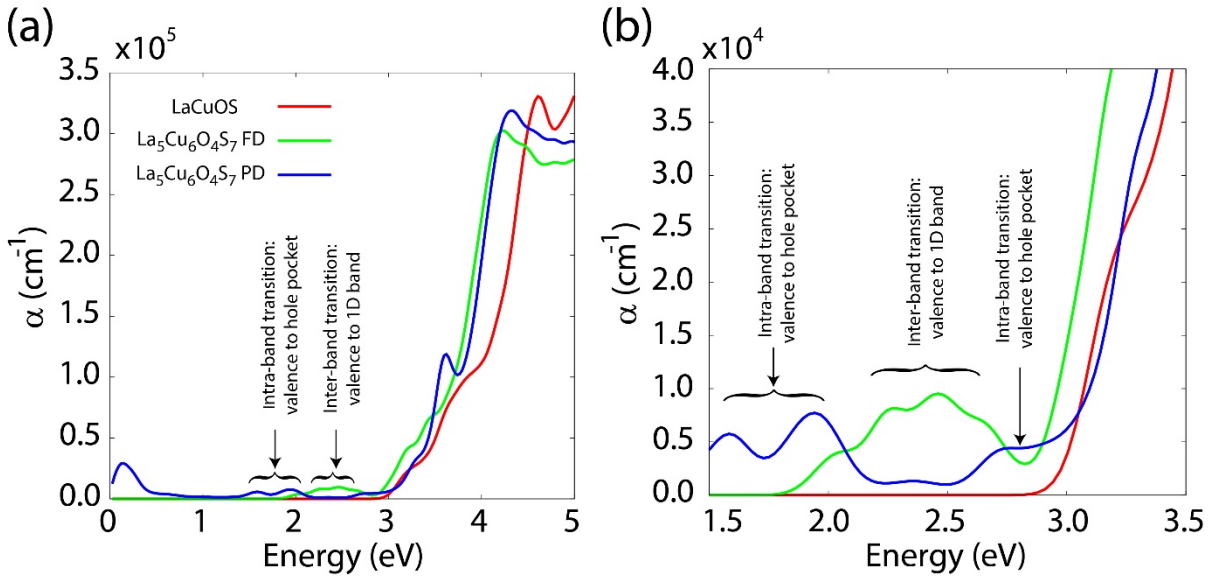

Figure 5. (a) Calculated optical absorption spectrum of $La_5Cu_6O_4S_7$ in the insulating fully dimerized (FD) configuration and in the lowest-energy partially dimerized configuration with dimer density x=0.66 compared to the absorption spectrum of LaCuOS. The optical absorption spectra of LaCuOS and of the misfit phases were calculated shifting the GGA conduction bands by an amount determined via an HSE06 calculation performed on a regular k-point grid. The HSE functional increases the valence-to-conduction energy distance at the Gamma point by 1.2 eV. (b) Zoom in on the absorption spectra displayed in panel (a) within the energy interval between 1.5 and 3.5 eV and showing the peak structure in the spectra of the two $La_5Cu_6O_4S_7$ phases close to the absorption threshold.